Anal Bioanal Chem (2011) 401:3125–3139
DOI 10.1007/s00216-011-5458-5

ORIGINAL PAPER

Nonpolar organic compounds in fine particles: quantification by thermal desorption–GC/MS and evidence for their significant oxidation in ambient aerosols in Hong Kong

Jian Zhen Yu · X. H. Hilda Huang · Steven S. H. Ho · Qijing Bian

Received: 9 May 2011 / Revised: 18 September 2011 / Accepted: 28 September 2011 / Published online: 11 October 2011

Abstract Nonpolar organic compounds (NPOCs) in ambient particulate matter (PM) commonly include *n*-alkanes, branched alkanes, hopanes and steranes, and polycyclic aromatic hydrocarbons (PAHs). The recent development of thermal desorption-gas chromatography/mass spectrometry (TD-GC/MS) has greatly reduced time and labor in their quantification by eliminating the laborious solvent extraction and sample concentration steps in the traditional approach that relies on solvent extraction. The simplicity of the TD-GCMS methods has afforded us concentration data of NPOCs in more than 90 aerosol samples in two aerosol field studies and 20 vehicular emissions-dominated source samples in Hong Kong over the past few years. In this work, we examine the interspecies relationships between select NPOCs and their concentration ratios to elemental carbon (EC) among the ambient samples and among the source samples. Our analysis indicates that hopanes were mainly from vehicular emissions and they were significantly oxidized in ambient PM. The hopane/EC ratio in ambient samples was on average less than half of the ratio in vehicular emissions-dominated source samples. This highlights the necessity in considering oxidation loss in applying organic tracer data in source apportionment studies. Select PAH/EC ratio–ratio plots reveal that PAHs had diverse sources and vehicular emissions were unlikely a dominant source for PAHs in Hong Kong. Biomass burning and other regional sources likely dominated ambient PAHs in Hong Kong.

Keywords Organic aerosols · Source apportionment · Molecular tracers · Atmospheric oxidation · Carbonaceous aerosol · Squalane

Published in the special issue *Aerosol Analysis* with guest editor Ralf Zimmermann.

J. Z. Yu · S. S. H. Ho
Department of Chemistry,
Hong Kong University of Science & Technology,
Clear Water Bay, Kowloon,
Hong Kong, China

J. Z. Yu (✉) · X. H. H. Huang · Q. Bian
Division of Environment,
Hong Kong University of Science & Technology,
Clear Water Bay, Kowloon,
Hong Kong, China
e-mail: chjianyu@ust.hk

S. S. H. Ho
SKLLQG, Institute of Earth Environment,
Chinese Academy of Sciences,
Xi'an 710075, China

Introduction

Sources of ambient organic aerosols (OA) come from both primary emissions and secondary formation in the atmosphere from oxidation of various volatile organic compounds. Identifying sources and quantifying their contributions is an essential initial step of air quality management. Ambient OA consists of numerous individual organic compounds [1]. Some of them are unique to certain aerosol sources and thereby can serve as tracers in source identification and apportionment [2]. Advances in receptor modeling have allowed source apportioning of organic aerosols without the need to gain a full characterization of the OA constituents [e.g., 3–5]. A number of nonpolar organic compounds (NPOCs) are among the commonly used tracers for primary OA sources.

NPOCs in ambient particulate matter (PM) commonly include *n*-alkanes, branched alkanes, hopanes and steranes (saturated cyclic hydrocarbons), and polycyclic aromatic hydrocarbons (PAHs). Hopanes and steranes, as part of unburned lubricating oil, are good indicators for vehicular emissions [2, 3, 6]; C_{29}–C_{31} odd alkanes are produced when leaves rub together in the wind, therefore serving as tracers for vegetative detritus; and C_{29}–C_{33} iso- and anteisoalkanes are identified to be tracers for cigarette smoke due to their presence as tobacco leaf wax [7–10]. Sources of PAHs are more diverse, with the ratio of some PAH pairs serving as a qualitative indicator for the dominance of a certain combustion sources [e.g., 11–14].

OA tracers have been traditionally analyzed using solvent extraction (SE) of filter samples followed by sample concentration and GC/MS (gas chromatography/mass spectrometric) analysis. The SE-GC/MS approach is labor intensive, therefore expensive. This in turns limits the number of samples that can be analyzed given limited resources. This constrain implies larger uncertainties in findings inferred from a spatially and temporally limited set of measurements.

We have developed an in-injection port thermal desorption–GC/MS (TD-GC/MS) analytical technique for NPOCs that significantly reduces the analysis time and the labor involved as a result of eliminating the sample pretreatment step [15, 16]. In our approach, small strips of aerosol-laden filter materials are packed into a GC injector liner. The NPOC species are thermally desorbed in the injection port and loaded onto the head of a GC column for subsequent separation and detection. Although the TD-GC/MS method could not entirely replace the more traditional solvent extraction-based method, the significant reduction in labor and in analysis time makes it possible to quantify nonpolar OA tracers for a larger number of samples for the same level of resources. This opens up the possibility of better understanding the atmospheric processing of the NPOC tracers and implications in their uses in source apportionment. Literature on the advancements and applications of thermal desorption in aerosol analysis has been summarized in two recent review reports [17, 18].

The in-injection port TD-GCMS method was deployed to quantify NPOCs in ~90 $PM_{2.5}$ (PM of smaller than 2.5 μm in aerodynamic diameter) ambient samples and 20 vehicular emissions-dominated source samples collected in Hong Kong. With this large NPOC data set, together with measurements of elemental carbon and other major aerosol constituents, we have examined interspecies relationships and applied the ratio–ratio plot approach developed by Robinson et al. [19, 20] to study the atmospheric processing of NPOC tracers and the implications on source identification and apportionment.

Experimental section

Samples

The collection details for the data sets of ambient and vehicular emissions-dominated sources are summarized in Table 1. All the ambient and tunnel PM samples were collected on pre-baked quartz fiber filters using samplers with a particle size cut of 2.5 μm in aerodynamic diameter.

The tunnel samples, nine of them, were collected in Shing Mun (SM) tunnel by a research team at the Hong Kong Polytechnic University. Details of the tunnel and sample collection can be found in a study report available from Hong Kong Environmental Protection Department [21] and in the paper by Ho et al. [22]. The tunnel does not have mechanical fresh air supply throughout their tubes. The sampling equipment was located near the cross-passageway of the tunnel. On average, approximately 47% of the total vehicles passing the tunnel during the sample collection period were diesel-fueled, 43% were gasoline-fueled, and the remaining were LPG vehicles. Eleven samples were collected at two roadside locations of heavy vehicular influence, Lok Ma Chau (LMC) and

Table 1 Description of PM2.5 samples used in this work

Sample set ID	No. of samples	Sampling location[a]	Sampling periods	Sampling flow rate and duration	Collection substrate
Tunnel samples	9	Shing Mun Tunnel	14 Jul.–6 Aug. 2003	55 Lmin^{-1} for 2 h	47 mm quartz fiber filters
Roadside samples	11	LMC and PU roadside	19–24 Jun. 2003 at PU site; 5–9 Jul. 2003 at LMC site	55 L min^{-1} for 3 h	47 mm quartz fiber filters
2006 summer samples	51	TC, TW, UST, YL	07 Jul.–01 Aug. 2006, once every other day sampling	1130 L min^{-1} for 24 h	20×25 cm quartz fiber filters
2010 winter samples	40	MK (roadside), TW, UST, YL	Nov. + Dec. 2010, once every six days sampling	1130 L min^{-1} for 24 h	20×25 cm quartz fiber filters

[a] Sampling location abbreviations: *LMC* Lok Ma Chau, *PU* Hong Kong Polytechnic University, *TC* Tung Chung, *TW* Tsuen Wan, *UST* Hong Kong University of Science and Technology, *YL* Yuen Long

Polytechnic University (PU). The samplers were placed on ground, with air intake point at ~1.3 m above ground. The LMC roadside site is located at the entrance of the boundary-crossing point where vehicles come from Mainland China to Hong Kong. The PU roadside site is located 1 m to a main road leading to the heavily used Cross Harbor Tunnel. PM collected at this site can represent street-level slow traffic emission exhausts when vehicles are idling and under slow traffic conditions.

Ambient $PM_{2.5}$ samples collected in two ambient field sampling campaigns were included in this work. The first campaign was conducted at four sampling locations in Hong Kong in the month of July 2006 with a sampling schedule of one 24-h sample every other day. The sampling sites include two locations in mixed residential and commercial neighborhood (TC and YL, see Table 1 for the full names of these two and other sampling sites), one urban location (TW), and one suburban location (UST). More details about this sampling campaign are given in our previous paper [23]. These samples, a total of 51 of them, are hereafter called 2006 summer samples. The second campaign was conducted at four sites in the months of November and December 2010 following a sampling schedule of one 24-h sample every six days. The sampling sites include the same three sites (TW, YL, and UST) used in the 2006 summer campaign and one downtown curbside location (MK). The MK site is located at the junction of heavily traffic roads in a downtown area. These samples, a total of 40 of them, are hereafter referred as 2010 winter samples. The sampling equipment at MK was on top of a 3-m high structure while at the other sites the samplers were located on building rooftops with heights 17–25 m above ground.

Chemical analysis

The NPOCs in the tunnel, roadside and ambient samples were analyzed using the in-injection port TD-GCMS method described in our previous papers [15, 16]. NPOCs targeted for quantification include C_{18}–C_{35} *n*-alkanes, C_{29}–C_{33} iso- and anteiso-alkanes, squalane, hopanes, PAHs of three- to seven-rings. Single standards of C_{18}–C_{20} alkanes and squalane were from Aldrich; C_{21}–C_{40} alkanes in a mixture were from Fluka. National Institute of Standards and Technology (NIST) SRM 2260A and SRM2266 were used as calibration standards for target PAHs and hopanes. The chromatograms of these target analytes are shown in Fig. 1.

Different amounts of filter materials were used for analysis in these samples as NPOC loading per square centimeter of exposed filter were different. A filter cut of 1 cm^2 was used for the tunnel and roadside samples while 3.0 and 2.0 cm^2 of filter materials were used for the 2006 summer samples and the 2010 winter samples, respectively. The analysis details have been described in our previous papers [15, 16]. Briefly, portions of quartz fiber filter samples were cut into smaller portions inserted into the TD tube, which was custom-fabricated to be the same dimensions as the Agilent 6890 GC (Santa Clara, CA, USA) split/splitless injector liner. The temperature of the injector port was lowered to 50 °C before analysis. The injector port temperature was then raised to 275 °C for desorption in a splitless mode while the GC oven temperature was kept at 30 °C. After the injector temperature reached 275 °C, the GC analysis began. The GC oven program was initially held at 30 °C for 2 min, increased to 120 °C at 10 °C min^{-1}, then to 310 °C at 8 °C min^{-1}, and finally held at 310 °C for 20 min. An HP-5 ms capillary column (5% diphenyl/95% dimethylsiloxane, 30 m×0.25 mm×0.25 μm, J&W Scientific, Folsom, CA, USA) was used. The MS was operated in scan mode from 50 to 650 amu. Identification was achieved by comparing the mass spectra and retention times of the chromatographic peaks with those of authentic standards. Quantification was based on peak area ratios of select fragment ions characteristic of individual NPOCs to those of internal standards [16].

All the samples were also analyzed for organic carbon (OC), EC and major ions. OC and EC were quantified using a thermal/optical transmittance method and the temperature protocol adopted was the Ace-Asia protocol [24], a protocol similar to the more commonly known NIOSH protocol [25, 26]. The major ions were quantified using IC and the method was described in Yang et al. [27].

Results and discussion

Advantages of the TD-GC/MS method

In comparison with the traditionally used SE-GC/MS approach, the TD-GC/MS has the prominent advantages of no need for sample pretreatment and that the amount of filter required for analysis is significantly reduced. Figure 2 shows the estimated amounts of filter material needed corresponding to different levels of NPOC air concentrations or loading per unit area (square centimeter) filter for the two methods. It is estimated that the SE-GC/MS method would require 45 times as much sampled filter materials as that required by the TD-GC/MS method. The difference is mainly due to that the sample utilization in the SE-GC/MS approach typically does not exceed 7% (i.e., 1 μL out of a final extract volume of 150 μL injected into the GC/MS). In making the estimation, the target amount of analyte per injection is set to be 1 ng/injection in the TD-GC/MS method and 0.3 ng/injection in the SE-GC/MS method. These values are approximately twice as much the reported

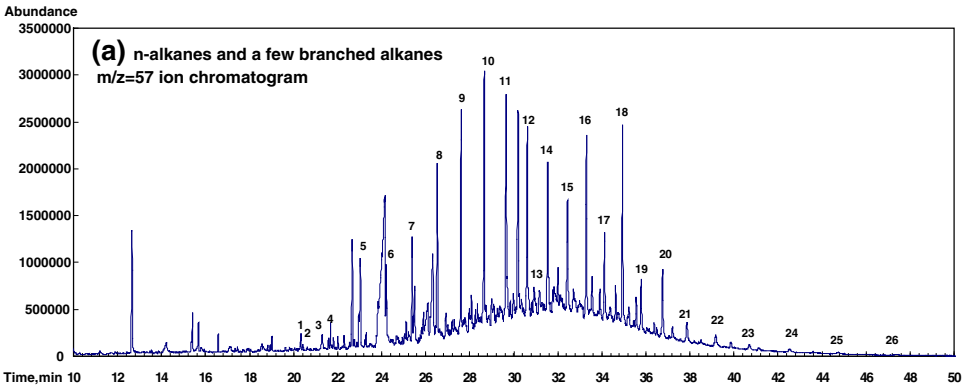

1.n-C17;2.pristane(C19);3.n-C18;4.phytane(C20);5.n-C19;6.n-C20;7.n-C21;8.n-C22;9.n-C23;10.n-C24;11.n-C25;12.n-C26;13.squalane(C30);14.n-C27;15.n-C28;16.n-C29;17.n-C30;18.n-C31;19.n-C32;20.n-C33;21.n-C34;22.n-C35;23.n-C36;24.n-C37;25.n-C38;26.n-C39.

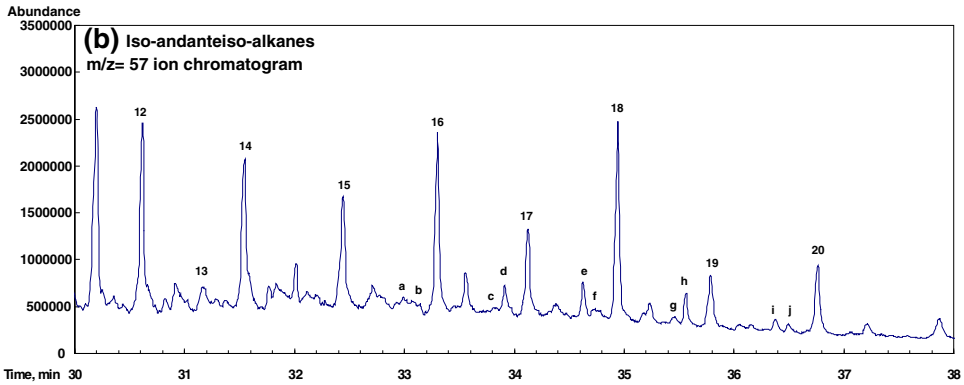

12.n-C26;13.squalane(C30);14. n-C27;15.n-C28;a.iso-C29;b.anteiso-C29;16.n-C29;c.iso-C30;d.anteiso-C30;17.n-C30;e.iso-C31;f.anteiso-C31;18.n-C31;g.iso-C32; h.anteiso-C32;19.n-C32;i.iso-C33;j.anteiso-C33;20.n-C33.

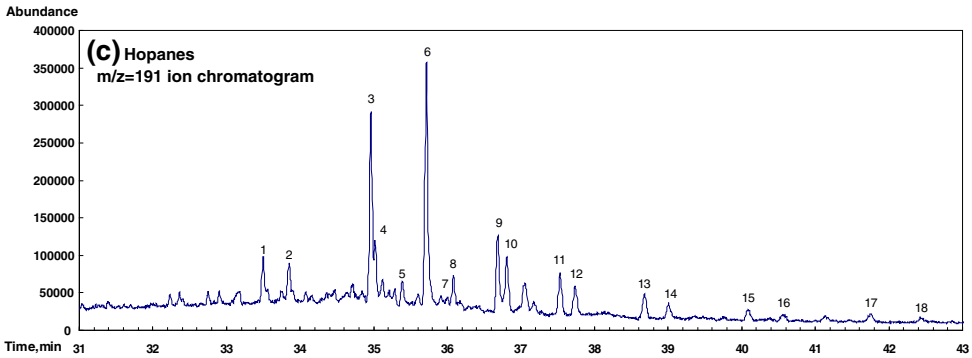

1.22,29,30-trisnorneophopane (27Ts); 2. 22,29,30-trisnorphopane (27Tm); 3. αβ-norhopane (C29); 4. 18α(H)-30-nor-neohopane (29Ts); 5. βα-norhopane + αα-norhopane (C29); 6. αβ-hopane (C30); 7. ααα-hopane (C30); 8. βα-hopane (C30); 9. αβS-homohopane (C31); 10. αβR-homohopane (C31); 11. αβS-bishomohopane (C32); 12. αβR-bishomohopane (C32); 13. 22S-trishomohopane (C33); 14. 22R-trishomohopane (C33); 15. 22Stetrahomohopane (C34); 16. 22R-tetrahomohopane (C34); 17. 22S-pentahomohopane (C35); 18. 22R-pentahomohopane (C35).

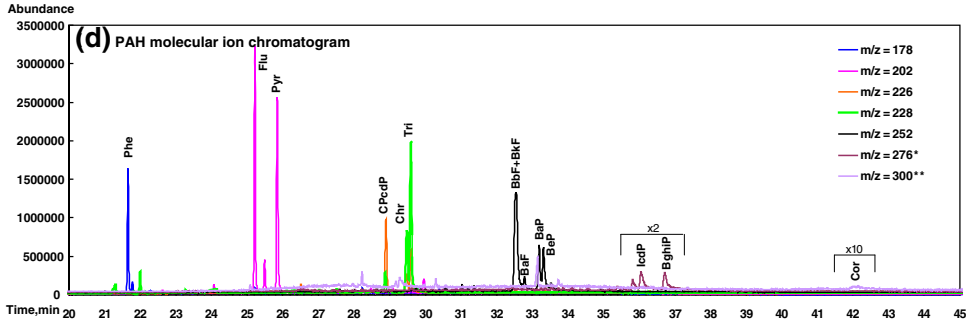

Species that are not included in Table 2: CPcdP - cyclopenta[cd]pyrene; Tri - triphenylene. * The responses of m/z = 276 are x 2. ** The responses of m/z = 300 are x 10.

Fig. 1 Example reconstructed ion chromatograms. **a** *n*-alkanes and a few branched alkanes, **b** Iso- and anteiso-alkanes, **c** Hopanes, and (**d**) PAHs. The abbreviations of PAHs are given in Table 2

limits of detection (LODs) for PAHs by the two methods [e.g., 13, 16]. The LODs of PAHs are typically ~0.3 ng/injection by the in-injection port TD-GC/MS method and 0.15–0.5 ng/injection by the SE-GC/MS method. Other NPOCs often exists at concentrations one order of magnitude higher than PAHs. Therefore, the ability to detect PAHs sets the limit for the amount of filter materials required. As shown by Fig. 2, if it is desired to quantify PAHs present at the level of 0.1 ng m^{-3}, approximately 2.5 cm^2 of filter materials sampled for 24 h by a high-volume sampler at 1.13 L m^{-3} are required for the TD-GC/MS analysis. In comparison, 114 cm^2 (approximately one-quarter of the entire high-volume filter) are needed for the SE-GC/MS analysis.

Figure 2 also offers a look-up diagram in determining the approximate amount of filter materials required for the TD-GC/MS and the SE-GC/MS methods.

Abundance of NPOCs in ambient and vehicular emissions-dominated source samples

Table 2 is a statistical summary of abundance of the target analytes in the urban atmosphere of Hong Kong and in the vehicular emissions-impacted source samples, reporting medians and ranges of the concentrations. It is noted that

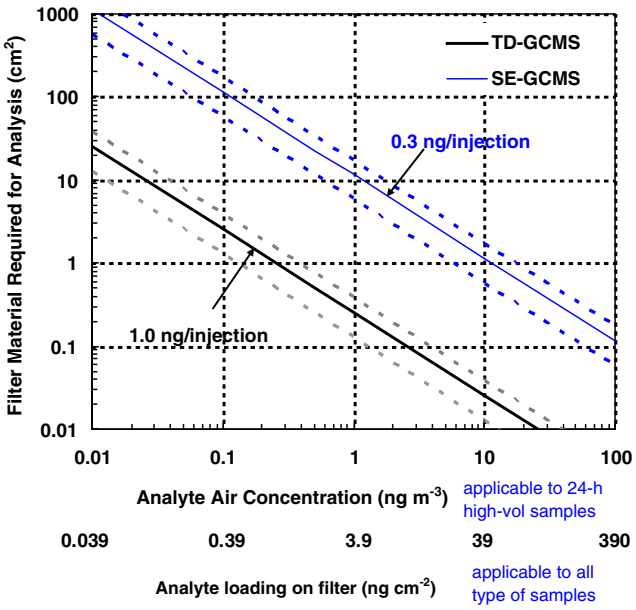

Fig. 2 Estimated amount of filter materials required in respect to target analyte air concentrations or loading per unit area of exposed filter. The following assumptions are made: (1) a sampled air volume is assumed to be 1,631 m^3, corresponding to 24 h sampling at a flow rate of 1.13 L min^{-1} by a $PM_{2.5}$ high-volume sampler. (2) For SE-GC/MS analysis, the final extract volume is assumed to be 150 μL and 1 μL is injected into the GCMS. (3) The *heavier lines* correspond to an assumed loading of 1.0 ng/injection for the TD-GC/MS analysis and 0.3 ng/injection for the SE-GC/MS analysis. The *dashed lines* correspond to ±50% the above assumed per injection amount

the different samplers deployed in the ambient sampling and source sampling resulted in different sampling face velocities (2.7 and 4.6 L min^{-1} cm^{-2}, respectively). Such a difference could bias the measured concentrations of the more volatile NPOCs by different degrees [28], adding to the measurement uncertainty. This source of sampling artifacts was recognized but no attempt was made to correct the reported measurements by the different samplers, as a quantitative relationship between this source of sampling artifacts and face velocity has not been established.

In terms of median concentrations, C_{18}–C_{33} *n*-alkanes are in the ranges of 0.2–7.2 ng m^{-3} in the ambient sample and 3.4–85 ng m^{-3} in the roadside samples, and 15–119 ng m^{-3} in the tunnel samples, reflecting that vehicular emissions are a significant source of particle-phase *n*-alkanes. The four most abundant hopanes are 17α(*H*), 21β(*H*)-29-norhopane (abbreviated as norhopane), 17α(*H*), 21β(*H*)-30-hopane (abbreviated as hopane), 17α(*H*), 21β(*H*)-22*S*-homohopane, and 17α(*H*), 21β(*H*)-22*R*-homohopane. Their median concentrations in the ambient samples (0.14–0.32 ng m^{-3}) are ~20 times lower than those in the roadside samples, which are approximately five times further lower than those in the tunnel samples. This order of hopane abundance is consistent with vehicular emissions being a known important source for hopanes. Sterane concentrations were typically low (<0.1 ng m^{-3}) or below detection limits in ambient samples. For this reason, they were not quantified in the 2006 summer samples and their concentrations in other sample groups are not reported here. The abundance of the 13 PAHs also has the concentration gradient from ambient samples (0.10–0.61 ng m^{-3}) to LMC and PU roadside samples (1.2–5.1 ng m^{-3}) to tunnel samples (3.0–40 ng m^{-3}); however, the concentration gradient among urban, roadside, and tunnel environments for the five- to seven-ring PAHs are not as stark as that observed for hopanes. The concentrations of three- and four-ring PAHs in the tunnel samples are significantly elevated in comparison with the roadside and the ambient samples. The concentrations of the five- to seven-ring PAHs in the tunnel samples are more than two times those in the roadside samples. An additional PAH compound, triphenylene, was quantified in the 2010 winter samples. Its concentration was in the range of 0.06–0.31 ng m^{-3}, with a mean concentration of 0.19 ng m^{-3}. This PAH is highly correlated to Chr (r^2=0.95, n=40), possibly suggesting common sources. Triphenylene was not included in the calibration standard mixtures in analysis prior to 2010 and consequently it was not quantified in other samples.

In the 2010 winter field campaign, a unique feature is that one of the four sampling sites (i.e., MK) is a location exposed to a significantly higher level of vehicle exhaust and sampling at this site was concurrent with the other three sites. This contrast in site characteristic provides conve-

Table 2 Statistical summary of abundance of NPOCs in two batches of ambient samples and in roadside samples collected in Hong Kong

	Abbreviation	LOD[a]	2006 Summer samples		2010 Winter samples		Roadside samples		Tunnel samples	
		ng/sample	Median	Range	Median	Range	Median	Range	Median	Range
PM2.5 ($\mu g/m^3$)			23	9.0–93.6	47	26–84	71	38–115	300	194–479
OC ($\mu g/m^3$)			3.3	1.0–14.2	13	6.1–20	14.3	7.8–24.6	53	35–66
EC ($\mu g/m^3$)			2.0	0.2–5.0	2.5	0.6–6.7	11	15–48	170	52–227
n-C_{18}–*n*-C_{26} alkanes		1.3–2.0	0.2–1.2	0.01–3.4	0.4–4.9	0.3–7.8	3.9–85	2.5–133	15–119	9–140
n-C_{27}–*n*-C_{33} odd alkanes		0.5–1.7	0.6–1.8	0.0–5.5	3.3–7.2	3.2–11.5	3.4–14	2.8–41	24–33	8.2–93
Iso- and anteiso-C_{29}–C_{33} alkanes		1.2–1.7	0.0–0.3	0.0–0.6	0.8–2.0	0.6–3.4	–[b]	–	–	–
Squalane		0.48	0.08	0.00–0.91	0.77	0.36–5.7	–	–	–	–
17α(*H*), 21β(*H*)-29-norhopane	Norhopane	0.15	0.20	0.03–0.6	0.31	0.06–1.3	6.5	3.6–20.0	36	19–43
17α(*H*), 21β(*H*)-30-hopane	Hopane	0.33	0.28	0.04–0.8	0.32	0.14–1.1	8.7	5.4–28.7	41	41–49
17α(*H*), 21β(*H*)-22*S*-homohopane	αβ*R*-homohopane	0.25	0.16	0.04–0.4	0.20	0.06–0.6	4.7	3.0–17.4	23	13–31
17α(*H*), 21β(*H*)-22*R*-homohopane	αβ*S*-homohopane	0.68	0.14	0.03–0.3	0.16	0.04–0.6	3.4	2.2–12.3	3.4	17–22
Phenanthrene	Phe	1.1	0.19	0.09–0.3	0.35	0.22–1.0	2.3	1.5–3.4	19	3.3–24
Fluoranthene	Flu	0.81	0.18	0.10–0.3	0.41	0.15–1.1	2.6	1.8–3.4	21	3.3–27
Pyrene	Pyr	0.91	0.60	0.48–0.9	0.46	0.16–1.0	3.6	2.0–5.2	40	6.3–51
Chrysene	Chr	0.24	0.28	0.24–0.3	0.29	0.06–0.5	2.0	1.1–3.4	3.8	2.0–4.7
Benzo[*b* + *k*]fluoranthene	BbF + BkF	0.36	0.79	0.06–1.28	0.67	0.55–0.92	5.1	1.1–10.2	16.2	4.4–21
Benzo[*a*]fluoranthene	BaF	0.22	–	–	0.19	0.16–0.25	1.8	1.6–2.3	1.8	2.6–3.6
Benzo[*e*]pyrene	BeP	0.66	0.14	0.02–0.20	0.25	0.17–0.35	4.2	0.8–7.0	11	3.4–15
Benzo[*a*]pyrene	BaP	0.67	0.22	0.02–0.37	0.60	0.48–0.88	1.4	0.2–4.4	8.3	1.0–10
Perylene	Pery	0.11	0.17	0.00–0.2	0.28	0.24–0.35	1.2	0.3–4.0	5.8	1.1–8.9
Indeno[1,2,3-*cd*]pyrene	IcdP	0.45	0.17	0.00–0.2	0.37	0.33–0.48	1.9	1.1–6.6	6.9	2.8–8.8
Benzo[*ghi*]perylene	BghiP	0.49	0.20	0.00–0.25	0.31	0.29–0.39	5.1	1.4–11.6	13	4.8–17
Coronene	Cor	0.44		0.00–0.32	0.18	0.00–0.20	4.6	1.8–8.2	10	4.5–14

[a] From Ho et al. [16]

[b] Not quantified due to low concentrations

nience in qualitatively assessing the importance of vehicular emissions to the ambient level of a given PM constituent by examining spatial variation. Figure 3 shows the spatial variation of hopanes, the sum of *n*-C_{29}–C_{33} odd alkanes, and a few PAHs, along with sulfate and EC. The lack of spatial variation in sulfate concentrations conforms its secondary formation nature (Fig. 3a) while the elevated EC levels at MK over the other sites were consistent with their site characteristics in respective to vehicular traffic (Fig. 3b). Among the NPOCs, hopanes showed the same spatial variation as EC did (Fig. 2c) while no concentration gradients were observed for C_{29}–C_{31} odd alkanes and PAHs. These spatial variation patterns indicate that vehicular emissions dominate the ambient concentrations of hopanes but are not a major source to ambient C_{29}–C_{31} odd alkanes and PAHs. It is noted that PAH levels in the LMC and PU roadside locations in 2003 were obviously higher than the ambient PAH levels in 2006 summer and 2010 winter samples (Table 2), contrast to observations at MK versus the other three ambient locations. This contrast could possibly be explained by different proximity to road traffic (3 m above ground at MK versus street-level at LMC and PU), change in vehicular emission profiles between the time of tunnel and LMC and PU roadside measurements (i.e., 2003) and the time of measurements in MK (i.e., 2010), and difference in vehicle composition and traffic volume at the three roadside locations. The "inconsistency" in the roadside PAH data also indicates that it is important to have the same timing and sampling strategies for ambient and source samples in planning future studies.

Source profiles of NPOCs in vehicular emissions

Vehicular emissions are invariably an important OA and fine PM source in any urban environments. As vehicle fleet composition and operation conditions vary from one city to another, source profiles of locally representative vehicular OA emissions are valuable in assessing contributions of

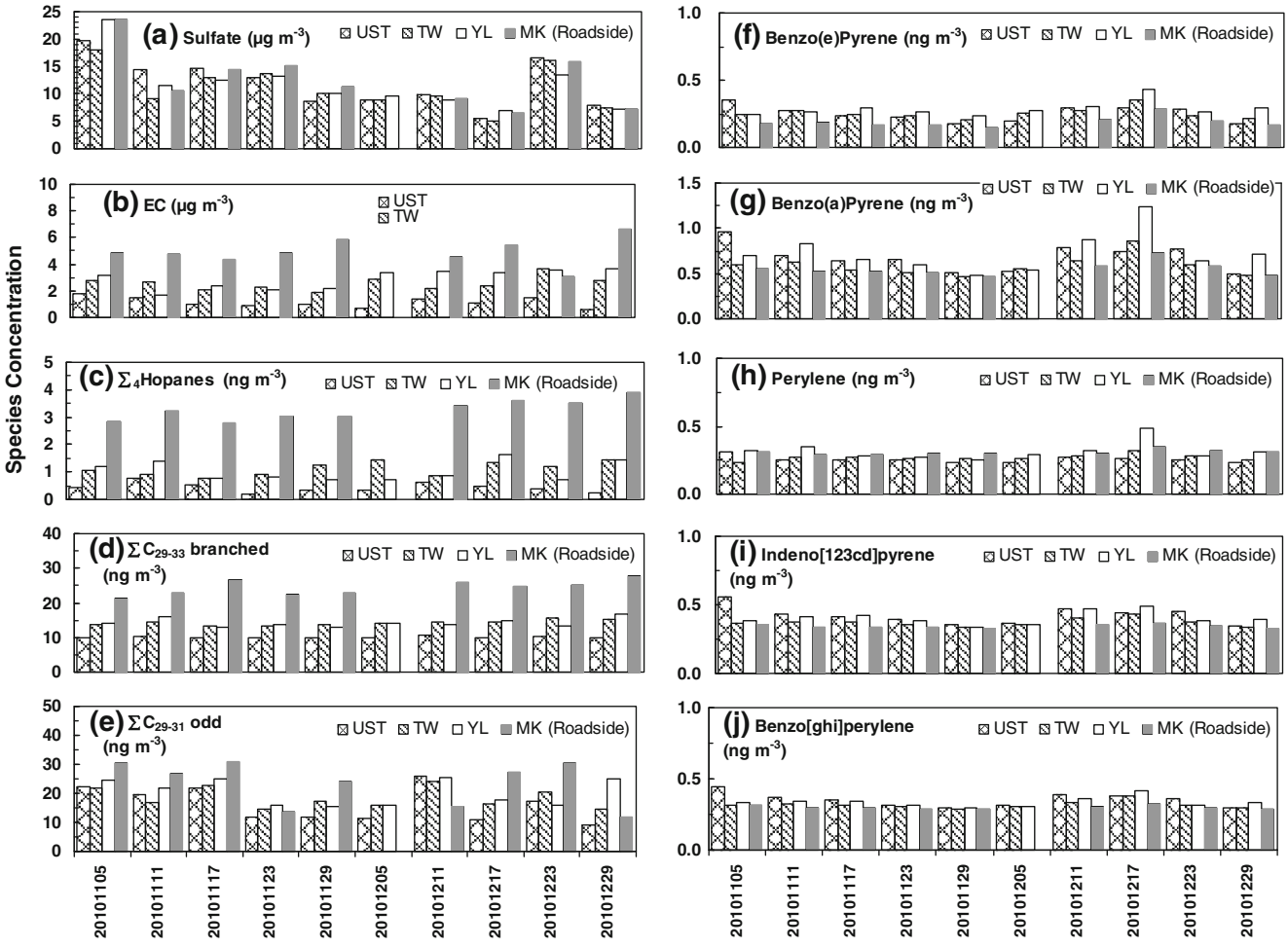

Fig. 3 Spatial variation of **a** sulfate, **b** EC, **c** sum of four hopane compounds, **d** sum of C_{29}–C_{33} branched alkanes, **e** sum of *n*-C_{29}–C_{33} odd alkanes, **f** benzo[*e*]pyrene, **g** benzo[*a*]pyrene, **h** perylene, **i** indeno[123*cd*]pyrene, and **j** benzo[*ghi*]perylene at four sites on ten sampling days in November and December 2010. One of the sampling sites (MK site) is a curbside location in a busy downtown district

vehicular emissions to ambient OA. For this reason, the NPOC source profile derived from the nine tunnel samples is compiled and shown in Table 3. We note that unresolved complex mixture, consisting of hundreds branched and cyclic alkanes that are not individually resolved by GC, constitutes a significant fraction of carbon mass in the vehicular emission OA. This source profile derived from tunnel snapshot of Hong Kong's vehicles also adds to the database of vehicular emission source profiles.

Hopanes and evidence for their significant oxidation in the ambient PM

The four most abundant hopanes are highly correlated in the data sets (r^2>0.8). Their relative abundance in either tunnel samples, or roadside samples, or ambient samples are similar. The proportion of norhopane: hopane : αβS-homohopane : αβ*R*-homohopane is 1.0:1.2:0.72:0.51 in the tunnel samples, 1.0:1.4:0.82:0.58 in the roadside samples, 1:1.3:0.67:0.56 in the 2006 summer samples, and 1:1.1:0.66:0.54 in the 2010 winter samples. The homohopane index [*S*/(*S* + *R*)] was 0.55 in the ambient data and 0.59 in the roadside and tunnel samples, in line with the typical value (0.6) for petroleum [29], rather than for coal smoke samples (0.05–0.35) [30]. The ratio of hopane to αβ*R*-homohopane was 2.1–2.3 in ambient samples, in line with the typical ratio for gasoline- and diesel-powered vehicle exhausts (2.2–2.9) [7]. In comparison, the typical ratios were 0.1–2.6 for coal smokes [30]. In summary, the relative proportions of hopane compounds and their spatial variation strongly suggest vehicular emissions dominate the ambient hopane levels. In the ambient samples, the sum of the four hopanes was found to positively correlate with EC (r^2=0.66 in the combined 2006 summer and 2010 winter data sets), further substantiating this suggestion.

An examination of the mass ratio between $\sum_4$hopanes and EC reveals that the ratio was 0.36 ng $\sum_4$hopanes/μg EC in the ambient samples, significantly lower than the ratio of 1.45±0.64 ng/μg derived from the samples collected in the tunnel and the two roadside locations. He et al. [31] reported a $\sum_4$hopanes/EC ratio of 1.14 ng/μg for emissions derived from a roadway tunnel in Guangzhou, a megacity ~100 km northwest to Hong Kong in the Pearl River Delta Region, close to our tunnel observation. The lower ratios in the ambient samples indicate faster loss of particle hopanes than EC in the atmosphere after their emissions.

Robinson et al. [19, 20] developed a ratio–ratio plot approach to visualize molecular tracer data in ambient data

Table 3 Vehicular emission source profile of nonpolar organic compounds derived from the tunnel samples (n=9)

Carbon	μgC/μg PM2.5	Hopanes	ng/μgC TC	PAHs	ng/μgC TC
TC	0.58±0.14	18α(*H*)-22,29,30-trisnorhopane (Ts)	0.12±0.05	Acenaphthylene	0.072±0.028
OC	0.16±0.03	17α(*H*)-22,29,30-trisnorhopane (Tm)	0.10±0.04	Acenapthene	0.009±0.004
EC	0.41±0.15	17α(*H*),21β(*H*)-30-norhopane (C29)	0.18±0.08	Fluorene	0.009±0.004
Alkanes	ng/μgC TC	18α(*H*)-30-nor-neohopane (C29)	0.03±0.02	Phenanthrene	0.064±0.027
UCM[a]	69±24	17β(*H*),21α (*H*)-30-norhopane (C29)	0.06±0.03	Anthracene	0.019±0.001
Octadecane (*n*-C18)	0.09±0.05	17α(*H*), 21β(*H*)-30-hopane (C30)	0.22±0.11	Fluoranthene	0.073±0.031
Nonadecane (*n*-C19)	0.12±0.04	17α(*H*), 21α(*H*)-30-hopane (C30)	0.01±0.01	Pyrene	0.141±0.062
Eicosane (*n*-C20)	0.22±0.09	17β(*H*), 21α(*H*)-30-hopane (C30)	0.05±0.02	Benzo[*a*]anthracene	0.019±0.005
Heneicosane (*n*-C21)	0.35±0.12	17α(*H*), 21β(*H*)-22*S*-homohopane (C31)	0.13±0.07	Chrysene	0.038±0.022
Docosane (*n*-C22)	0.54±0.16	17α(*H*), 21β(*H*)-22*R*-homohopane (C31)	0.091±0.050	Benzo[*b*+*k*]fluoranthene	0.063±0.016
Tricosane (*n*-C23)	0.62±0.16	17α(*H*), 21β(*H*)-22*S*-bishomohopane (C32)	0.065±0.036	Benzo[*a*]fluoranthene	0.019±0.008
Tetracosane (*n*-C24)	0.62±0.19	17α(*H*), 21β(*H*)-22*R*-bishomohopane (C32)	0.041±0.024	Benzo[*e*]pyrene	0.048±0.011
Pentacosane (*n*-C25)	0.53±0.22	22*S*-trishomohopane (C33)	0.035±0.022	Benzo[*a*]pyrene	0.028±0.012
Hexacosane (*n*-C26)	0.27±0.14	22*R*-trishomohopane (C33)	0.019±0.012	Perylene	0.024±0.010
Heptacosane (*n*-C27)	0.17±0.09	22*S*-tretrahomohopane (C34)	0.014±0.009	Indeno[1,2,3-*cd*]pyrene	0.031±0.003
Octacosane (*n*-C28)	0.17±0.12	221-tetrashomohopane (C34)	0.009±0.006	Dibenzo[*a*,*h*]anthracene	0.032±0.008
Nonacosane (C-29)	0.16±0.12	22*S*-pentashomohopane(C35)	0.016±0.010	Benzo[*ghi*]perylene	0.059±0.013
Triacontane (*n*-C30)	0.17±0.09	22*R*-pentashomohopane(C35)	0.009±0.005	Coronene	0.054±0.011
Hentriacotane (*n*-C31)	0.18±0.11				
Dotriacontane (*n*-C32)	0.17±0.12				
Tritriactotane (*n*-C33)	0.22±0.15				
Tetratriactoane (*n*-C34)	0.20±0.13				

[a] Unresolved complex mixture

and source profiles in one single plot. In the ratio–ratio plots, two molecular tracers are normalized against a common non-reactive aerosol species (e.g., EC). If there is a single source dominating the ambient concentrations of the molecular tracers, then photochemical decay will cause the ambient data to be distributed along a line in a ratio–ratio plot originating from the source profile [20].

Figure 4 shows the ratio–ratio plot of hopane and norhopane normalized by EC for the ambient, roadside and tunnel samples, along with the ratios in published emission source profiles of industrial coal combustion, gasoline-powered and diesel-powered engines [32–36]. Of the two vehicular sources, diesel-powered vehicles are important sources of both EC and hopanes while gasoline-powered vehicles are important sources of hopanes but minor contributors to EC. Consequently, the ratios of hopane to EC are significantly lower in diesel-powered vehicles than gasoline-powered vehicles. The average norhopane/EC and hopane/EC ratios in different sample groups are (0.32, 0.42) in the tunnel samples, (0.35, 0.47) in the LMC and PU roadside locations, (0.26, 0.20) in the MK roadside location, (0.11, 0.15) in the 2010 winter samples, and (0.09, 0.12) in the 2006 summer samples. As seen from Fig. 4, the tunnel/roadside data and ambient data appear to be distributed along a diagonal line that emanates from the gasoline source profile point in the upper-right corner toward the lower-left-hand corner of the plot. The majority ambient data are distributed away from the tunnel/roadside data and further towards the lower-left-hand corner. More than two-thirds of the ambient data have higher hopane/EC ratios than the diesel source profile. Such a pattern in the ratio–ratio plot identifies gasoline-powered engines as the dominant source for the hopane compounds and also indicates their significant photochemical oxidation in the ambient environment after their emissions. Substantial oxidation of hopanes was also observed in the ambient environment of Pittsburgh [37] and later demonstrated through exposing aerosolized motor oil to hydroxyl radical in smog chamber experiments [38, 39].

It is noted that there was no discernable difference in the extent of hopane oxidation between the 2006 Summer samples and the 2010 winter samples. This contrasts with the higher extent of oxidation observed in Pittsburg in the summer than in the winter [19]. In Hong Kong, the summer–winter contrast in photooxidation activity is not as stark due to its subtropical location. In addition, the high relative humidity conditions (typically >70%) in the summer inhibits the OH oxidation, as found in smog chamber experiments [38, 39]. The combined result of the above two factors may explain the lack of seasonality in the condensed-phase hopane oxidation in Hong Kong.

Hopanes and EC are the key species for apportioning gasoline and diesel emissions in the commonly used chemical mass balance (CMB) model for source apportionment. Zheng et al. [4] performed CMB analysis on a molecular marker data set derived from $PM_{2.5}$ samples collected in Hong Kong in four sampling months representative of four seasons in an annual cycle from November 2000 to October 2001 in Hong Kong. The CMB analysis apportions negligible contributions to ambient OA from gasoline-powered vehicles at an urban site (TW) and a rural site. Such an unexpected result indicates that CMB underestimated gasoline vehicle contributions, which is an expected outcome of assuming hopanes are chemically stable. This illustrates the importance of recognizing the significant oxidation of hopanes in source apportionment studies.

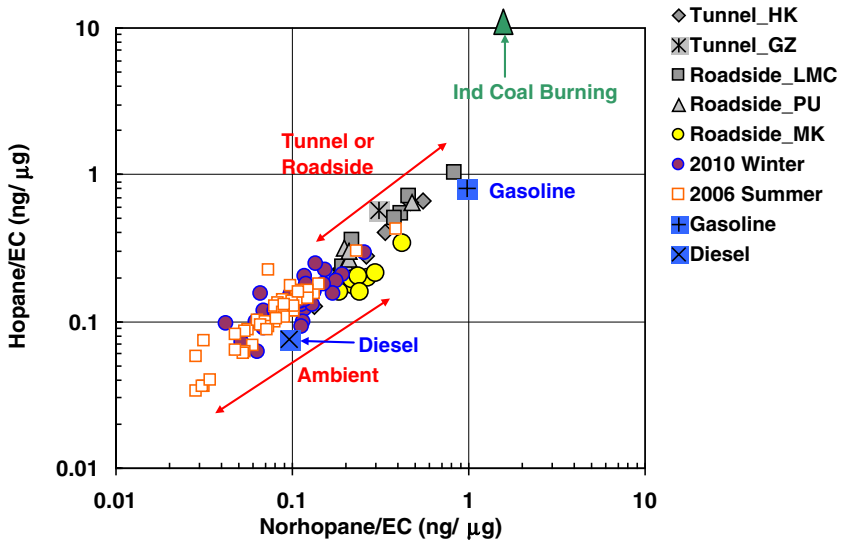

Fig. 4 Ratio–ratio plot of hopane and norhopane normalized by EC for both ambient, tunnel and roadside samples collected in Hong Kong. Also shown are emission ratios for source samples include industrial coal cobustion, gasoline- and diesel-powered vehicular emissions, tunnel source profile from Guangzhou (*Tunnel_GZ*) [31]. The ratios in source profiles of industrial coal combustion [36] are off-scale. The gasoline and diesel profiles are averages of a number of published vehicle profiles [7, 32–35]

PAHs

PAHs are the products of incomplete combustion from various sources. Fossil fuel combustion, including diesel and gasoline combustion in vehicles, industrial coal combustion for power generation, and biomass burning are expected to be significant combustion sources in our study region.

Molecular diagnostic ratios have been commonly used to infer PAH emission sources [e.g., 11–14]. Ambient ratios of a certain pair of PAHs are compared with source ratios of the same pair of PAHs. If the ambient ratio is close to the ratio in a known source, then it is implied that this source has a dominant influence on the ambient PAH levels. In this PAH ratio approach, the PAH pairs typically have similar molecular size (e.g., BaP and BeP, BghiP and IcdP, Flu and Pyr, Phe and Ant, see Table 2 for the definitions of PAH abbreviations). The use of ratio has the advantage of canceling out variation of particle-phase concentration due to temperature change (which strongly influences gas–particle partitioning, especially for three- and four-ring PAHs) and chemical degradation. However, source ratios often rely on limited measurements. The ratios for different combustion sources are not always sufficiently different. For example, BghiP/IcdP ratio was 0.6–1.4 in industrial coal burning emissions [36] and 0.8 in rice straw burning emissions [40]. For this reason, we here use scatter plot and ratio–ratio plots to identify dominating sources [20].

Among the quantified PAHs, five-ring and larger PAHs are generally positively correlated in the ambient samples; certain three- and four-ring PAHs (e.g., Phe, Ant, Flu, Pyr, and Chr) also display positive correlations. As the three- and four-ring PAHs have considerable presence in both gas and aerosol phases and the gas–particle partition shifts as ambient temperature changes, this complicates the comparison of particle-phase PAHs between tunnel samples collected in the summer and the ambient samples, which were collected in both summer and winter. We therefore focus the source analysis on the five-ring and larger PAHs since the majority of these larger PAHs mainly reside in the

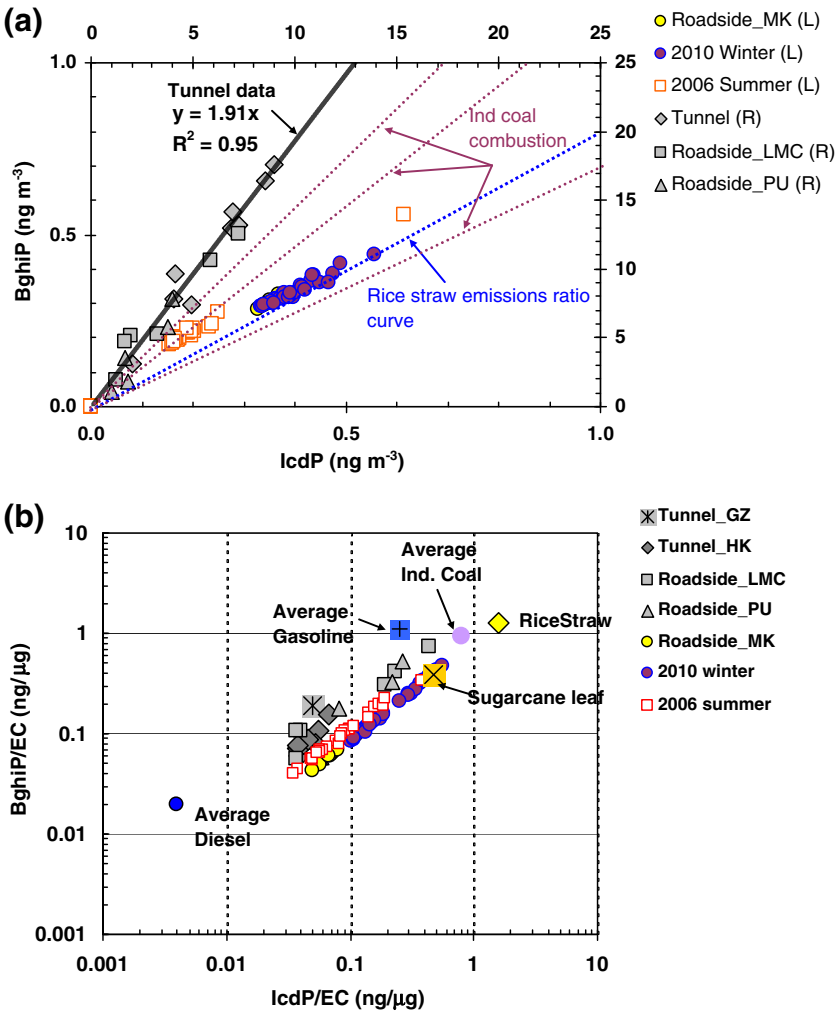

Fig. 5 BghiP vs. IcdP. **a** Scatter plot of BghiP and IcdP concentrations in tunnel, roadside and ambient samples. Note different concentration scales (marked *R* and *L* to denote *right* and *left scales*) are applied to the ambient data and the source data. **b** Ratio–ratio plot normalized by EC. Also shown in the ratio–ratio plots are emission ratios for source samples include industrial coal cobustion, gasoline- and diesel-powered vehicular emissions, tunnel in Guangzhou, and biomass burning emissions. The gasoline and diesel profiles are averages of a number of published vehicle profiles [7, 32–35]. The tunnel in Guangzhou data was from He et al. [31]. The rice straw and sugarcane burning emission profiles were obtained from $PM_{2.5}$ samples collected near open field burning in our study region

particle-phase under typical ambient summer and winter temperatures [41].

A scatter plot of BghiP versus IcdP in the ambient, roadside and tunnel samples is displayed in Fig. 5a, with ambient data distributed along one line and the tunnel/roadside data forming a separate line. The strong correlations between the two PAHs suggest a common set of sources dominates their ambient concentrations. The significant deviation of the ambient line (summer data slope, 1.0; winter data slope, 0.83) from the tunnel-derived vehicular source profile (slope, 1.9) indicates that vehicles were not the dominant source for the two PAHs in the ambient environment of Hong Kong. The slope of the 2010 winter ambient line at the value of 0.83 is similar to the BghiP/IcdP ratio (0.8) in rice straw burning emissions obtained in open field burning in our region [40] and in dilution chamber measurements of simulated rice straw burning [42]. The 2006 summer ambient line slope (1.0) is larger than the winter ambient ratio and rice straaw burning source ratio, indicating that dominant sources of the two PAHs are different in the two seasons. The BghiP/IcdP ratio in industrial coal combustion was in the range of 0.6–1.4, bracketing the ambient ratios.

The ratio–ratio plot of the two PAHs normalized by EC is shown in Fig. 5b, along with emission ratios for average industrial coal combustion [36], average gasoline and diesel [24], rice straw and sugarcane leaf burning in this region [40]. It appears that the domiance of either industrial coal combustion or the common form of biomass burning in this region, in combination of photochemical oxidation, could explain the ambient data distribution in the ratio–ratio plot.

Similar analysis is performed on anothor two PAHs, BaP and BeP, to examine their dominant sources (Fig. 6). Strong correlations of BaP and BeP in the ambient samples exist (r^2>0.65; Fig. 6a). The summer data are more scattered. The two PAHs form two separate lines among the ambient summer and winter data, indicating their dominant sources are season-dependent. The slope values of the ambient data (winter, 2.5; summer, 1.5) are significantly higher than the BaP/BeP ratio (0.66) derived from the tunnel samples, as

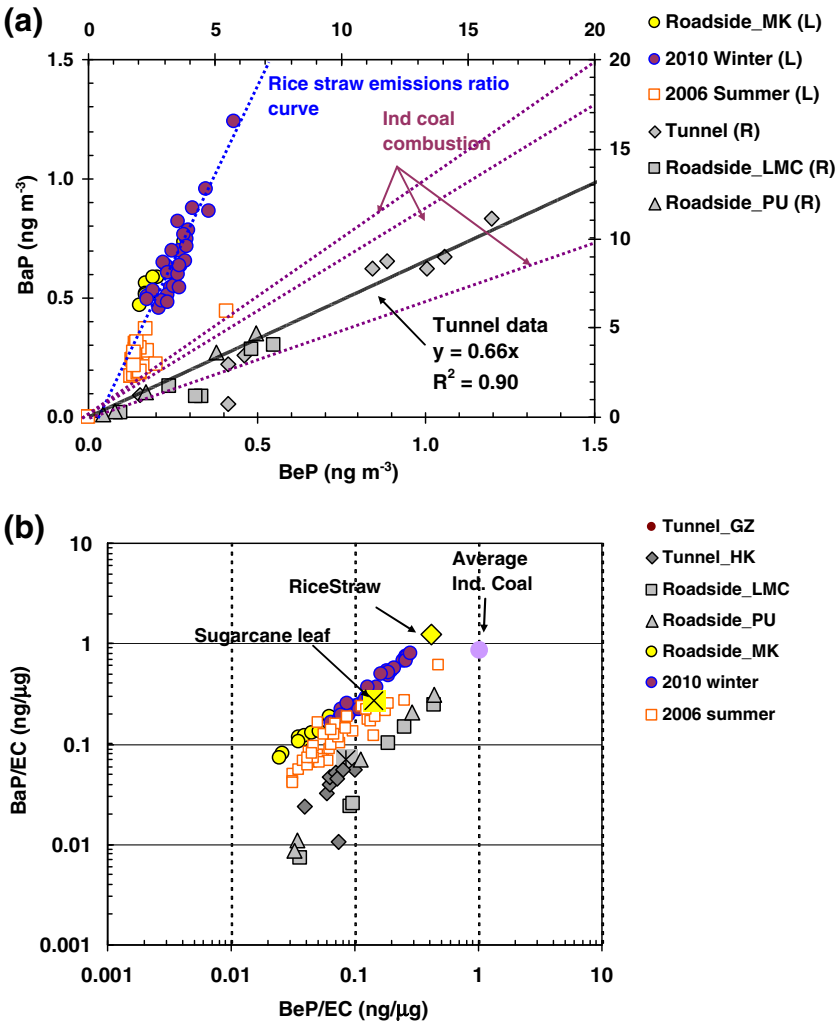

Fig. 6 BaP vs. BeP. **a** Scatter plot of BaP and BeP concentrations in tunnel, roadside and ambient samples. Note that different concentration scales are applied to the ambient and source data. **b** Ratio–ratio plot normalized by EC. Also shown in the ratio–ratio plots are emission ratios for source samples include industrial coal cobustion [36] and biomass burning emissions. The rice straw and sugarcane burning emission profiles were obtained from $PM_{2.5}$ samples collected near open field burning in our region

well as the ratio range of 0.5–1.0 reported for industrial coal combustion [36]. The winter ambient ratio was close to, but slightly lower than the ratio (2.9) representing rice straw burning emissions.

The ratio–ratio plot of BaP and BeP normalized by EC (Fig. 6b) shows that the summer ambient data had lower BaP/EC than the winter ambient data. BaP and BeP are structural isomers but BaP is photochemically more unstable than BeP. BaP has a half life of 5.3 h under strong sunlight conditions, while BeP has a half life of 21.1 h which is stable to photolysis [43, 44]. The lower BaP/EC in summer ambient data may be partially due to photolytic degradation of BaP. More than half of the roadside samples had higher ratios of BaP and BeP to EC than the tunnel samples, indicating even for roadside locations other sources could dominate the cncentrations of BaP and BeP. The ratio plot indicates that sources such as rice straw burning and industrial coal combustion, in combination with atmospheric oxidation, could explain the BaP and BeP ambient data; however, this does not exclude some other sources serving as the dominant source.

C_{29}, C_{31}, and C_{33} odd alkanes

C_{29}–C_{33} odd alkanes are highly correlated (r^2>0.85) in both ambient and tunnel/roadside samples. The ratio–ratio plot of n-C_{29} and n-C_{31} alkanes normalized by EC is shown in Fig. 7a. Unlike the ratio–ratio plot of norhopane and hopane (Fig. 4), the ambient data of n-C_{29} and n-C_{31} alkanes are distributed in the upper-right-hand corner above the vehicular emissions source data, clearly indicating that the odd alkanes are dominated by sources other than vehicular emissions. This is consistent with our knowledge that vegetative detritus, an OA source without accompa-

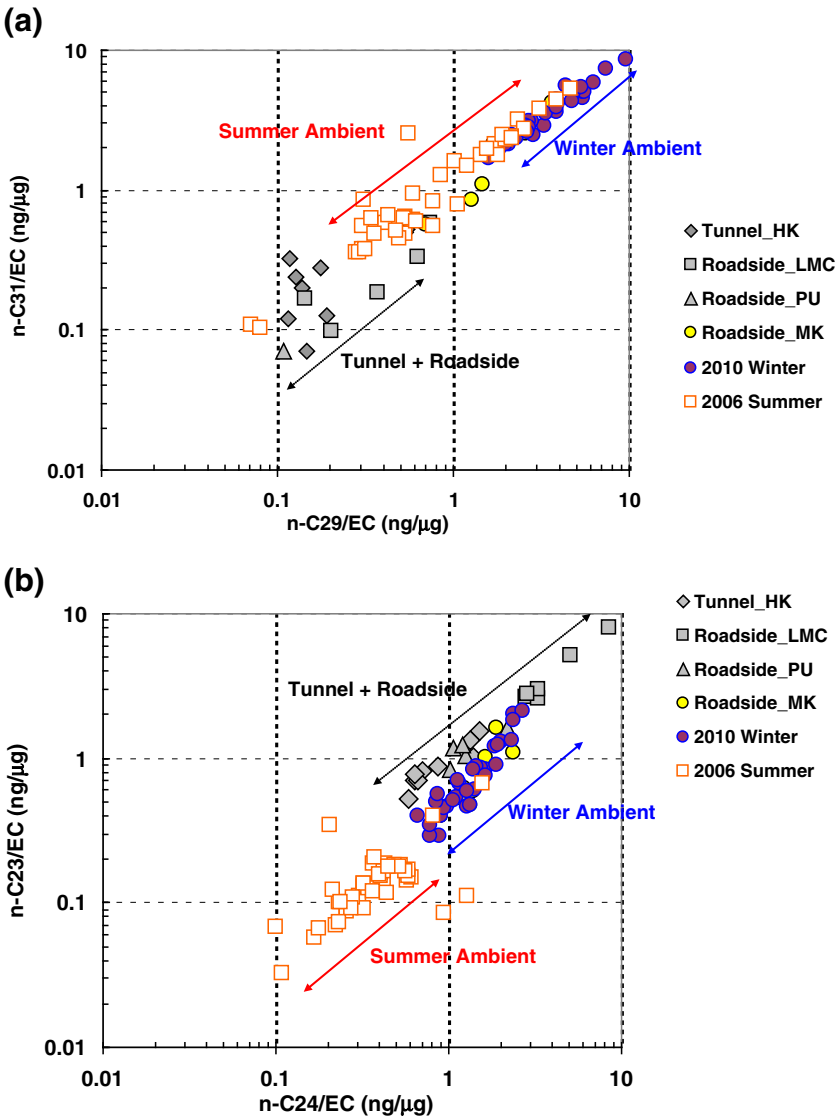

Fig. 7 **a** Ratio–ratio plot of n-C_{31} and n-C_{29} alkanes normalized by EC; **b** ratio–ratio plot of n-C_{23} and n-C_{24} alkanes nomalized by EC

nying EC, is the known main source of these high molecular weight odd alkanes [8].

For comparison purposes, a ratio–ratio plot of n-C_{23} and n-C_{24} alkanes normalized by EC is shown in Fig. 7b. These two alkanes are known to be associated with fossil fuel use. They are semi-volatile, consequently their particle-phase concentrations are expected to be strongly dependent on ambient temperature. We note that the tunnel data were collected on summer days. Therefore, while the summer ambient data could be compared with the tunnel data, the winter ambient data would be biased towards higher ratio values due to a shift of the gas–particle partitioning towards the particle phase. In the ratio–ratio plot, the 2010 winter ambient data are clustered together with the tunnel/roadside data in the upper-right-hand corner of the plot while the 2006 summer ambient data are distributed in the lower-left-hand corner on the same line formed by the winter ambient data and the tunnel/roadside data. Two points could be made from this figure. First, the ratio–ratio plot is consistent with vehicular emissions being the dominant source of n-C_{23} and n-C_{24} alkanes. Second, significant atmospheric oxidation of the two alkanes is evident in the summer ambient environment.

Squalane

Squalane has recently been used as a model hydrophobic compound in the aerosol phase in the study of OH aging of aerosols [e.g., 44–47]. Its ambient concentrations are rarely reported in the literature. Its concentrations were found to show a strong spatial gradient, highest at MK (downtown roadside; average: 3.8 ng m^{-3}) and significantly lower at the other sampling locations (average, 0.7 ng m^{-3}). Squalane positively correlates with hopanes, n-C_{28}, n-C_{30}, n-C_{32} alkanes, iso- and anteiso-alkanes (r^2>0.65) in the 2010 winter samples. Squalane is a natural hydrocarbon and triterpene derived from a variety of plant and animal sources. The major sources for aerosol squalane have yet to be investigated and identified.

Conclusions

In-injection port thermal desorption GC/MS provides a simple method in quantifying nonpolar organic compounds in aerosol samples. Its simplicity and need for much smaller amount of aerosol materials than the traditionally solvent extraction GC/MS approach makes feasible the analysis of NPOCs in greater numbers of aerosol samples. This results in improved and more representative temporal and spatial data coverage, which in turn reduce uncertainty in data intepretation in relation of their sources and atmospheric chemistry.

We have explored NPOC measurements in more than 90 ambient samples and 20 vehicular emissions-dominated source samples collected in Hong Kong. The focus NPOCs are those that serve as tracers for ambient OA sources. Spatial variation pattern confirms hopanes to be primarily from vehicular emissions. Their ratios to EC in the ambient data in comparison with those in the tunnel and roadside samples reveal that significant atmospheric oxidation after their emissions had occurred in Hong Kong's urban atmosphere. The important implications of this finding is that source contributions to gasoline vehicles would be underestimated without consideration of the atmospheric oxidation of hopane in tracer-based source apportionment.

Comparison of the ambient data and the tunnel/roadside data also leads to the conclusion that the ambient concentrations of the larger PAHs, such as BaP, BeP, BghiP, IcdP, are not dominated by vehicular emissions. Sources such as rice straw burning and industrial coal combustions are more likely the dominant sources for these PAHs in Hong Kong.

Acknowledgments This project is partially supported by Hong Kong Environment Protection Department (AS 03-399 and AS 10-131) and the Research Grants Council of Hong Kong, China (622409). We thank Dr. Peter Louie for initiating the sampling efforts in Hong Kong during the 2006 summer PRD field measurement campaign and the Hong Kong Environmental Protection Department for logistics support in our field campaigns. We also thank Professor Frank S. C. Lee and his team for collecting the tunnel and roadside samples.

References

1. Schnelle-Kreis JW, Welthagen M, Sklorz R, Zimmermann R (2005) Application of direct thermal desorption gas chromatography and comprehensive two-dimensional gas chromatography coupled to time of flight mass spectrometry for analysis of organic compounds in ambient aerosol particles. J Sep Sci 28:1648–1657
2. Cass GR (1998) Organic molecular tracers for particulate air pollution sources. Tr Anal Chem 17:356–366
3. Schauer JJ, Rogge WF, Hildemann LM, Mazurek MA, Cass GR (1996) Source apportionment of airborne particulate matter using organic compounds as tracers. Atmos Environ 30:3837–3855
4. Zheng M, Hagler GSW, Ke M, Bergin MH, Wang F, Louie PPK, Salmon L, Sin DWM, Yu JZ, Schauer JJ (2006) Composition and sources of carbonaceous aerosols at three contrasting sites in Hong Kong. J Geophys Res 111:D20313. doi:10.1029/2006JD007074
5. Hu D, Bian QJ, Lau AKH, Yu JZ (2010) Source apportioning of primary and secondary organic carbon in summer PM2.5 in Hong Kong using positive matrix factorization of secondary and primary organic tracer data. J Geophys Res 115:D16204. doi:10.1029/2009JD012498
6. Simoneit BRT (1984) Organic-matter of the troposphere. 3. Characterization and sources of petroleum and pyrogenic residues in aerosols over the western United States. Atmos Environ 18:51–67
7. Rogge WF, Hildemann LM, Mazurek MA, Cass GR, Simoneit BRT (1993) Sources of fine organic aerosol. 2. Noncatalyst and catalyst- equipped automobiles and heavy-duty diesel trucks. Environ Sci Technol 27:636–651

8. Rogge WF, Hildemann LM, Mazurek MA, Cass GR, Simoneit BRT (1993) Sources of fine organic aerosol. 4. Particulate abrasion products from leaf surfaces of urban plants. Environ Sci Technol 27:2700–2711
9. Rogge WF, Hildemann LM, Mazurek MA, Cass GR, Simoneit BRT (1993) Sources of fine organic aerosol. 6. Cigarette smoke in the urban atmosphere. Environ Sci Technol 28:1375–1388
10. Bi XH, Sheng GY, Feng YL, Fu JM, Xie JX (2005) Gas- and particulate-phase specific tracer and toxic organic compounds in environmental tobacco smoke. Chemosphere 61:1512–1522
11. Khalili NR, Scheff PA, Holsen TM (1995) PAH source fingerprints for coke ovens, diesel and gasoline engines, highway tunnels, and wood combustion emissions. Atmos Envr 29:533–542
12. Sienra M, del R, Rosazza NG, Préndez M (2005) Polycyclic aromatic hydrocarbons and their molecular diagnostic ratios in urban atmospheric respirable particulate matter. Atmos Res 75:267–281
13. Tan JH, Bi XH, Duan JC, Rahn KA, Sheng GY, Fo JM (2006) Seasonal variation of particulate polycylic aromatic hydrocarbons associated with PM10 in Guangzhou, China. Atmos Res 80:250–262
14. Evagelopoulos V, Albanis TA, Asvesta A, Zoras S (2010) Polycylic aAromatic hydrocarbons (PAHs) in fine and coarse particles. Global NEST J 12:63–70
15. Ho SSH, Yu JZ (2004) In-injection port thermal desorption and subsequent gas chromatography–mass spectrometric analysis of polycyclic aromatic hydrocarbons and *n*-alkanes in atmospheric aerosol samples. J Chromatogr A 1059:121–129
16. Ho SSH, Yu JZ, Chow JC, Zielinska B, Watsona JG, Sit EHL, Schauer JJ (2008) Evaluation of an in-injection port thermal desorption-gas chromatography/mass spectrometry method for analysis of non-polar organic compounds in ambient aerosol samples. J Chromatogr A 1200:217–227
17. Chow JC, Yu JZ, Watson JG, Ho SHH, Bohannan TL, Hays MD, Fung K (2007) The application of thermal methods for determining chemical composition of carbonaceous aerosols: a review. J Environ Sci Health, Part A 42:1521–1541
18. Hays MD, Lavrich RJ (2007) Developments in direct thermal extraction-GC/MS of fine aerosols. Trends Anal Chem 26:88–102
19. Robinson AL, Donahue NM, Rogge WF (2006) Photochemical oxidation and changes in molecular composition of organic aerosol in the regional context. J Geophys Res 111:D03302. doi:10.1029/2005JD006265
20. Robinson AL, Subramanian R, Donahue NM, Bernardo-Bricker A, Rogge WF (2006) Source apportionment of molecular markers and organic aerosols 1. Polycyclic aromatic hydrocarbons and methodology for data visualization. Environ Sci Technol 40:7803–7810
21. Hong Kong Polytechnic University (2005) Determination of suspended particulate & VOC emission profiles for vehicular sources in Hong Kong. http://www.epd.gov.hk/epd/english/environmentinhk/air/studyrpts/files/1-pt_final_report_20050225d.pdf. Accessed 14 September 2011
22. Ho KF, Lee SC, Ho WK, Blake DR, Cheng Y, Li YS, Ho SSH, Fung K, Louie PKK, Park D (2009) Vehicular emission of volatile organic compounds (VOCs) from a tunnel study in Hong Kong. Atoms Chem Phys 9:7491–7504
23. Hu D, Bian Q, Li TWY, Lau AKH, Yu JZ (2008) Contributions of isoprene, monoterpenes, β-caryophyllene, and toluene to secondary organic aerosols in Hong Kong during the summer of 2006. J Geophys Res 113:D22206. doi:10.1029/2008JD010437
24. Schauer JJ, Mader BT, Deminter JT, Heidemann G, Bae MS, Seinfeld JH, Flagan RC, Cary RA, Smith D, Huebert BJ, Bertram T, Howell S, Kline JT, Quinn P, Bates T, Turpin B, Lim HJ, Yu JZ, Yang H, Keywood MD (2003) ACE-Asia intercomparison of a thermal-optical method for the determination of particle-phase organic and elemental carbon. Environ Sci Technol 37:993–1001
25. Birch ME, Cary RA (1996) Elemental carbon-based method for monitoring occupational exposures to particulate diesel exhaust. Aerosol Sci Technol 25:221–241
26. NIOSH (1999) Method 5040 Issue 3 (Interim): Elemental carbon (diesel exhaust). In: NIOSH manual of analytical methods, 4th edn. National Institute of Occupational Safety and Health, Cincinnati
27. Yang H, Yu JZ, Ho SSH, Xu JH, Wu WS, Wan CH, Wang XD, Wang XR, Wang LS (2005) The chemical composition of inorganic and carbonaceous materials in PM2.5 in Nanjing, China. Atmos Environ 39:3735–3749
28. McDow SR, Huntzicker JJ (1990) Vapor adsorption artifact in the sampling of organic aerosol-face velocity effects. Atmos Environ 24A:2563–2571
29. Seifert WK, Moldowan JM (1978) Applications of steranes, terpanes, and monoaromatics to the maturation, migration, and source of crude oils. Geochim Cosmochimica Acta 42:77–95
30. Oros DR, Simoneit BRT (2000) Identification and emission rates of molecular tracers in coal smoke particulate matter. Fuel 79:515–536
31. He LY, Hu M, Zhang YH, Huang XF, Yau TT (2008) Fine particle emissions from on-road vehicles in the Zhujiang Tunnel, China. Environ Sci Technol 42:4461–4466
32. Schauer JJ, Kleeman MJ, Cass GR, Simoneit BRT (1999) Measurement of emissions from air pollution sources. 2. C-1 through C-30 organic compounds from medium duty diesel trucks. Environ Sci Technol 33:1578–1587
33. Schauer JJ, Kleeman MJ, Cass GR, Simoneit BRT (2002) Measurement of emissions from air pollution sources. 5. C-1-C-32 organic compounds from gasoline-powered motor vehicles. Environ Sci Technol 36:1169–1180
34. Fraser MP, Lakshmanan K, Fritz SG, Ubanwa B (2002) Variation in composition of fine particulate emissions from heavy-duty diesel vehicles. J Geophys Res 107:8346. doi:10.1029/2001JD000558
35. Watson JG, Fujita EM, Chow JC, Zielinska B (1998) Northern Front Range Air Quality Study final report and supplemental volumes. Desert Res. Inst, Reno
36. Zhang YX, Schauer JJ, Zhang YH, Zeng LM, Wei YJ, Liu Y, Shao M (2008) Characteristics of particulate carbon emissions from real-world Chinese coal combustion. Environ Sci Technol 42:5068–5073
37. Subramanian R, Donahue NM, Bernardo-Bricker A, Rogge WF, Robinson AL (2006) Contribution of motor vehicle emissions to organic carbon and fine particle mass in Pittsburgh, Pennsylvania: effects of varying source profiles and seasonal trends in ambient marker concentrations. Atmos Environ 40:8002–8019
38. Weitkamp EA, Lambe AT, Donahue NM, Robinson AL (2008) Laboratory measurements of the heterogeneous oxidation of condensed-phase organic molecular markers for motor vehicle exhaust. Environ Sci Technol 42:7950–7956
39. Lambe AT, Miracolo MA, Henningan CI, Robinson AL, Donahue DM (2009) Effective rate constants and uptake coefficients for the reactions of organic molecular markers (*n*-alkanes, hopanes, and steranes) in motor oil and diesel primary organic aerosols with hydroxyl radicals. Environ Sci Technol 43:8794–8800
40. Yu H, Yu JZ (2011) Size distributions of polycyclic aromatic hydrocarbons at two receptor sites in the Pearl River Delta Region, China: implications of a dominant droplet mode. Aerosol Sci Tech 45:101–112
41. Yang Y, Guo P, Zhang Q, Li D, Zhao L, Mu D (2010) Seasonal variation, sources and gas/particle partitioning of polycyclic aromatic hydrocarbons in Guangzhou, China. Sci Total Environ 408:2492–2500

42. Sheesley RJ, Schauer JJ, Chowdhury Z, Cass GR, Simoneit BRT (2003) Characterization of organic aerosols emitted from the combustion of biomass indigenous to South Asia. J Geophys Res 108:4285. doi:10.1029/2002JD002981
43. Katz M, Chan C, Tosine H, Sakuma T (1979) Relative rates of photochemical and biological oxidation (in vitro) of polynuclear aromatic hydrocarbons. In: Jones PW, Leber P (eds) Polynuclear aromatic hydrocarbons. Ann Arbor Science, Ann Arbor, pp 171–189
44. Panther BC, Hooper MA, Tapper NJ (1999) A comparison of air particulate matter and associated polycyclic aromatic hydrocarbons in some tropical and temperate urban environments. Atmos Environ 33:4087–4099
45. Che DL, Smith JD, Leone SR, Ahmed M (2009) Quantifying the reactive uptake of OH by organic aerosols in a continuous flow stirred tank reactor. Phys Chem Chem Phys 11:7885–7895
46. Kroll JH, Smith JD, Che DL, Kessler SH, Worsnop DR, Wilson KR (2009) Measurement of fragmentation and functionalization pathways in the heterogeneous oxidation of oxidized organic aerosol. Phys Chem Chem Phys 11:8005–8014
47. Smith JD, Kroll JH, Cappa CD, Che DL, Liu CL, Ahmed M, Leone SR, Worsnop DR, Wilson KR (2009) The heterogeneous reaction of hydroxyl radicals with sub-micron squalane particles: a model system for understanding the oxidative aging of ambient aerosols. Atmos Chem Phys 9:3209–3222